Astronomy & Astrophysics

LETTER TO THE EDITOR

Discovery of thermal X-ray emission in the supernova remnant G337.8−0.1 (Kes 41)

J. A. Combi[1,3], J. F. Albacete-Colombo[2,3], and J. Martí[1]

[1] Departamento de Física (EPS), Universidad de Jaén, Campus Las Lagunillas s/n, A3, 23071 Jaén, Spain
   e-mail: [jcombi;jmarti]@ujaen.es
[2] Centro Universitario Regional Zona Atlántica (CURZA). Universidad Nacional del COMAHUE, Monseñor Esandi y Ayacucho (8500), Viedma (Rio Negro), Argentina
   e-mail: donfaca@gmail.com
[3] Facultad de Ciencias Astronómicas y Geofísicas, Universidad Nacional de La Plata, Paseo del Bosque, B1900FWA La Plata, Argentina

ABSTRACT

Aims. We report here on the first detection at X-ray wavelengths of the Supernova Remnant (SNR) G337.8−0.1, carried out with the XMM-*Newton* Observatory.
Methods. Using the X-ray observations, we studied the X-ray morphology of the remnant at different energy ranges, analysed the spectral properties and investigated a possible variable behavior.
Results. The SNR shows a diffuse filled-center structure in the X-ray region with an absence of a compact source in its center. We find a high column density of $N_{\rm H} > 6.9 \times 10^{22}$ cm^{-2}, which supports a relatively distant location ($d \geq 7$ kpc). The X-ray spectrum exhibits emission lines, indicating that the X-ray emission has a thin thermal plasma origin, and is well represented by a non-equilibrium ionization (NEI) plasma model. The X-ray characteristics and well-known radio parameters show that G337.8−0.1 belongs to the emerging class of mixed-morphology (MM) SNRs.

Key words. ISM: supernova remnants – ISM: individual object: G337.8−0.1 – X-rays: ISM

1. Introduction

G337.8−0.1 (also known as Kes 41) was discovered with the Molonglo telescope at 408 MHz (Shaver & Goss 1970). This object, located in the southern galactic plane, was reported in the Molonglo Observatory Synthesis Telescope (MOST) Catalog (Whiteoak & Green 1996) as a bright small-diameter SNR and distorted shell. The remnant is $6' \times 9'$ in size, distinctly elongated in the northeast-southwest direction. Based on HI observations, Caswell et al. (1975) placed the SNR beyond the tangent point at 7.9 kpc. Koralesky et al. (1998) detected maser emission in the object at −45 km s^{-1}, implying a far kinematic distance of 12.4 kpc. This fact is characteristic of a shock interaction with dense molecular gas (Green et al. 1997). The MOST flux density of $S_{\rm 843\ MHz} = 18$ Jy, combined with $S_{\rm 408\ MHz} = 26$ Jy (Shaver & Goss 1970), gives a spectral index of $\alpha \sim -0.51$ for the remnant.

At X-ray frequencies the object was never detected by early X-ray missions. This non-detection is likely a result of the absorption of the typically soft (i.e., <2 keV) X-ray emission by the high column density of gas and dust in the Galactic plane. As a part of an effort to identify and study the X-ray emission of the SNR G337.8−0.1 we have used the greatly enhanced X-ray sensitivity provided by the XMM-*Newton* telescope. An instrument with these characteristics offers a unique opportunity to study heavily obscured SNRs.

In this Letter we report the first detection at X-ray wavelengths of SNR G337.8−0.1. The object is characterized by an apparent centrally brightened X-ray morphology and a spectrum which suggests that the bright central emission is thermal in nature. The structure of the paper is as follows: in Sect. 2 we describe the XMM-*Newton* observations and data reduction. X-ray analysis and results are presented in Sect. 3. In Sect. 4 we discuss the implications of our results and summarize the main conclusions.

2. Observations and data reduction

The SNR G337.8−0.1 was observed on September 2005 by the XMM-*Newton* X-ray satellite (Obs-Id. 0303100101). The observation was centered towards the source ($\alpha_{\rm J2000.0} = 16^{\rm h}39^{\rm m}06\!\!.^{\rm s}5$, $\delta_{\rm J2000.0} = -46°57'58\!\!.''0$), and images were acquired with the EPIC MOS (Turner 2001) and EPIC PN (Strüder et al. 2001) cameras. The observation was made through a "*thin*" filter, and in the full frame (FF) imaging mode. The observation was retrieved from the XMM-Newton Science Archive (XSA)[1], and raw EPIC data were calibrated using the last version of the Standard Analysis System (SAS-V7.1.2)[2]. To construct images, spectra and light curves, we selected events with FLAG==0, and PATTERNS ≤ 12 and 4 for the MOS and PN cameras, respectively.

We derive Good Time Intervals (GTI) by the accumulation of background light-curves in the 10–15 keV energy band, which leads to a reduction of ~15% in the net exposure time of the observation. The net exposure time of the observation for all EPIC cameras finally reaches about 44.8 ks. Unfortunately, the

---

[1] http://xmm.vilspa.esa.es/xsa/
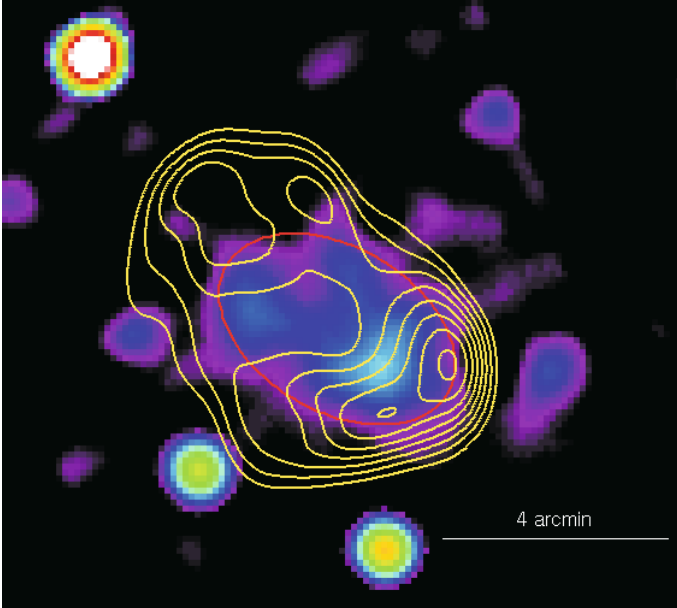[2] http://xmm.vilspa.esa.es/external/xmm_sw_cal/sas.shtml

Fig. 1. XMM-*Newton* image of Kes 41 in the 0.5–10 keV energy range. The radio map observed with the MOST at 843 MHz is over-lapped in yellow contours (Whiteoak & Green 1996). Radio contours are indicated in steps of 0.2, 0.29, 0.38, 0.47, 0.56, 0.65, 0.74 and 0.83 mJy beam^{-1}. The resolution is ~43″ × 43″ cosec (δ). The red el-lipse shows the region from which the X-ray spectra was extracted (see Sect. 3.2).

object was negatively affected by bad columns and CCD gaps in the EPIC-PN camera, which makes the spatial and spectral study of the X-ray emission from the SNR unreliable. In order to avoid systematics that affect the reliability of our analysis, we made use of only the EPIC-MOS1/2 data.

3. X-ray analysis of G337.8−0.1

3.1. Image

We use the clean event files to generate MOS1 and MOS2 im-ages in the energy band [0.5–10] keV with a spatial binning of 6.53 arcsec per pixel. In order to increase the signal-to-noise (S/N) ratio, we use the *emosaic* SAS task to merge the two MOS1/2 images. The corresponding set of exposure maps for each camera was prepared to account for spatial quantum effi-ciency and mirror vignetting by running the SAS task *eexmap*. Exposure vignetting corrections were performed by dividing the superposed count image by the corresponding superposed expo-sure maps. We adaptively smoothed this to a S/N ratio of 10 using the SAS task *asmooth*.

Figure 1 shows the X-ray image of the SNR G337.8−0.1 in the 0.5–10.0 keV energy band with the radio contours at 843 MHz superposed. The image reveals diffuse X-ray emission with an apparent filled-center structure and the absence of a com-pact source in its center. The X-ray peak of the SNR G337.8−0.1 is located at ($\alpha_{J2000.0} = 16^h38^m55^s.7$, $\delta_{J2000.0} = -46°58'32''.4$), and as can be seen, the X-ray emission region is smaller than the radio structure. In fact, the X-ray emission fills the interior of the radio shell and lies mainly in the southwest part of the radio shell.

To examine the morphology of the remnant in more detail, we have generated narrow-band images in the energy ranges 0.5–2 keV, 2–4 keV, 4–6 keV and 6–10 keV. In Fig. 2 we show the images in the four narrow energy bands. The source is
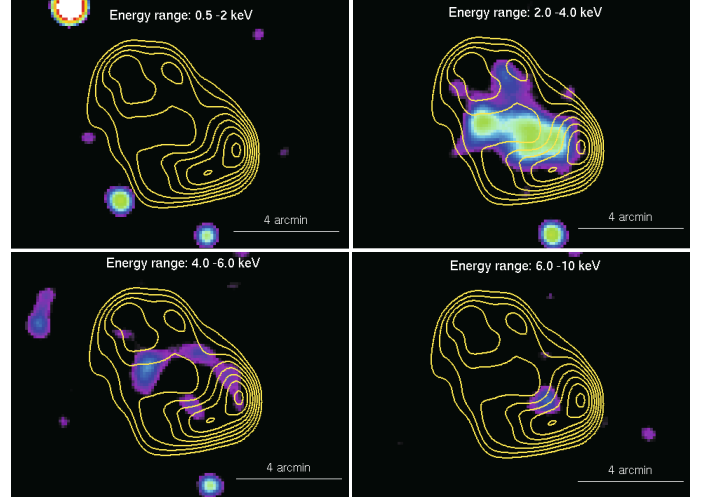

Fig. 2. Composite XMM-*Newton* images of G337.8−0.1 at low, me-dian and high energy (0.5–2 keV, 2–4 keV, 4–6 keV, 6–10 keV) for the combined MOS1/2 cameras. Note the lack of soft X-ray photons in the 0.5–2 keV energy range, while mostly of the X-ray emission is clearly observed in the 2–4 keV image and the semi-circular structure in the 4–6 keV band.

almost undetected below 2 keV. The distribution of the emis-sion in the 2–6 keV range is quite similar to the broadband image. The centroid of the hard X-ray emission lies in the SW region of the remnant. The absorbed X-ray fluxes for the bands are: $F_{0.5-2\ keV} = 1.3 \times 10^{-14}$ erg s^{-1} cm^{-2}, $F_{2-4\ keV} = 1.6 \times 10^{-13}$ erg s^{-1} cm^{-2}, $F_{4-6\ keV} = 7.35 \times 10^{-14}$ erg s^{-1} cm^{-2} and $F_{6-10\ keV} = 2.9 \times 10^{-14}$ erg s^{-1} cm^{-2}, which correspond to 5%, 58%, 26% and 11% of the total X-ray emission, respectively. As can be seen, mostly of the X-ray emission originates in the 2–6 keV band.

3.2. Spectral analysis

For the spectral analysis we used MOS1/2 data. It was performed using the XSPEC package (Arnaud 1996). Since the statistics of the source is not complete enough to perform a spatial resolved spectral analysis, we extracted X-ray photon events for the whole source by using an elliptical region with a major axis of 5 arcmin and a minor axis of 3.2 arcmin, as indicated in Fig. 1. The background region was taken from a nearby blank region in the neighborhood of the source. Ancillary response files (ARFs) and redistribution matrix files (RMFs) were calculated. The spectra were grouped with a minimum of 12 counts per bin. The background-subtracted spectra of the MOS data are shown in Fig. 3. At high X-ray energies (above 6 keV), the spectra show features with low statistical significance (~1 to 1.5 sigma), and are probably related to fluorescence lines in the background spectrum of the XMM-*Newton* (e.g. De Luca & Molendi 2004).

Our analysis of the XMM-*Newton* EPIC spectra was per-formed using a NEI model (Mazzotta et al. 1998) (see Fig. 3). The model was affected by a multiplicative absorption WABS (WABS$_{ISM}$ + WABS$_{SNR}$) model (Morrison & McCammon 1983). The goodness of the model fit was derived according to the χ^2-test statistics. C-statistics was also applied to the spectral fit, giving similar results. Results of the spectral analysis are sum-marized in Table 1. The presence of excess soft emission is not surprising, given that Kes 41 is located in a crowded region of the galaxy at a distance of between 7 to 12 kpc. Emission-line fea-tures corresponding to the blend of S XV and Si XIV are clearly
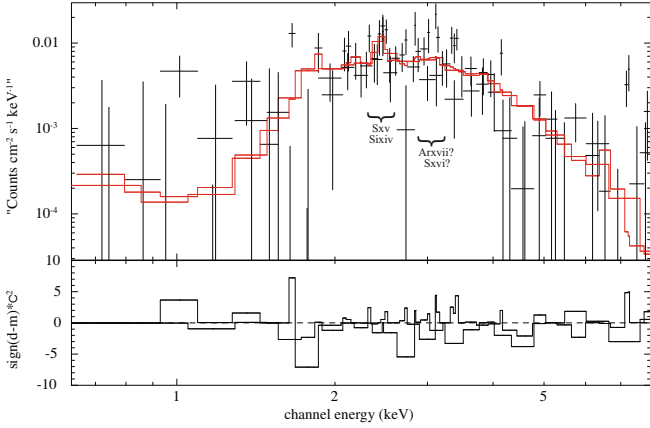
Fig. 3. The XMM-*Newton* MOS1/2 spectrum of the diffuse X-ray emission of Kes 41. The solid line indicates the best fit for the NEI model (see Table 1). The soft X-ray excess are probably due to foreground emission. The position of the most intense transition lines of S XV and Si XIV elements are indicated. The total number of photons is 3725 and 2539 for MOS1 and MOS2, respectively.

Table 1. X-ray spectral parameters of the SNR G337.8-0.1.

| Model: | NEI | |
Parameter	Value	1σ error
N_H^{ISM} [cm^{-2}]	2.2×10^{22}	fixed
N_H^{SNR} [cm^{-2}]	4.7×10^{22}	1.0×10^{22}
kT [keV]	1.4	0.2
Abundance[†]	0.6	0.3
$\log(\tau)$ [s cm^{-3}]	11.0	0.3
Normalization	3.4×10^{-3}	1.1×10^{-3}
Flux [erg cm^{-2} s^{-1}]	7.5×10^{-12}	1.8×10^{-12}
χ^2/ν-d.o.f.	1.08/380	–

Notes: the ISM H I absorption column density (N_H^{ISM}) was computed by following Dickey & Lockman (1990) HI in the Galaxy, and kept fixed in the fit procedure. The logarithm of ionization timescale $\log(\tau)$ is also written as $\log(n_e t)$. Flux is absorption-corrected in the 0.5–10.0 keV energy range. Normalization was calculated according to: $10^{-14}/4\pi r^2 \int n_e n_H dV$. [†] The abundance was adopted from Anders & Grevesse (1989) and left as a free parameter in all our fits.

visible at ~2.4 keV. Possible detection of others elements like Ar XVII and S XVI emission lines appear blended around 3.1 keV. Although the presence of these lines support a thermal nature for the X-ray emission, the absence of significant Fe XXV at 6.7 keV does not allow us to discard a weak non-thermal contribution at high X-ray energies.

To obtain a statistical assessment of the X-ray variability of the SNR G337.8−0.1, we use the 44.8 ks EPIC-PN observation to compare the time arrival distribution of source photons by means of the Kolmogorov-Smirnov (KS) test (Press et al. 1992). We use an extraction region centered on the whole X-ray emission. We see no significant pulsed signal with a period greater than twice the read-out time of the EPIC-PN camera in the FF mode (73.3 ms), which corresponds to a Nyquist limit of 0.146 s. At first glance, the absence of any significant X-ray variability and a thermal origin for the X-ray emission allows us to discard an energetic pulsar associated with the SNR.

4. Discussion

The SNR G337.8−0.1 is characterized by an apparent centrally filled X-ray morphology not well correlated with the radio shell,

and thermally dominated X-ray emission. Thus, Kes 41 could be classified as a thermal composite (or mixed-morphology) remnant. Moreover, at radio frequencies, the emission is non-thermal (Whiteoak & Green 1996) and can be interpreted as synchrotron radiation from accelerated high-energy electrons at the SNR shock. These characteristics place the remnant in the emerging class of SNR that includes objects such as W44 (Jones et al. 1993), 3C 391 (Rho & Petre 1996); G272.2−3.2 (Harrus et al. 2001) and G290.1−0.8 (Slane et al. 2002). A list containing SNRs with these characteristics was proposed by Rho & Petre (1998).

Although the evolutionary states that led to the observed properties in these SNRs is not well understood, it is widely believed that these peculiar characteristics are linked to inhomogeneities in the ISM. Several possible scenarios have been introduced in the past to explain thermal X-ray radiation inside radio shells of SNRs, i) cloudlet evaporation in the SNR interior (White & Long 1991); ii) thermal conduction smoothing out the temperature gradient across the SNR and enhancing the central density (Cox et al. 1999); iii) a radiatively cooled rim with a hot interior (Harrus et al. 1997); and iv) possible collisions with molecular clouds (Safi-Harb et al. 2005).

G337.8−0.1 lies in a complex region of the sky, possibly adjacent to a very massive giant molecular cloud (Dame et al. 1986) and close to the associated maser emission detected at −45 km s^{-1} by Koralesky et al. (1998). If the SNR is indeed propagating in a region with a large number of clouds, the most suitable scenario for describing the SNR evolution is that developed by White & Long (1991). In such remnants, the clouds evaporate by saturated conduction (Cowie & McKee 1977) and the X-ray morphologies may be very different from ordinary shell-like SNRs.

Based on the X-ray properties of G337.8−0.1, specifically the filled-center morphology and detected lines in the spectrum, a thermal interpretation of the X-ray emission is the most plausible to describe the SNR evolution. Using the X-ray image of G337.8−0.1 we estimated the volume V of the X-ray emitting plasma, assuming that the plasma fills an ellipsoid similar to the region from which the X-ray spectra was extracted (with a diameter of $5' \times 3'.2$). For a distance range from 7 to 12 kpc, we then obtained a volume of $(2.8–14.8) \times 10^{58}$ cm^3. Based on the emission measure (EM) determined by the spectral fitting, we can estimate the electron density of the plasma, n_e, by $n_e = \sqrt{EM/V}$, which varies between 0.20 cm^{-3} and 0.26 cm^{-3}. In this case, the number density of the nucleons was simply assumed to be the same as that of electrons. The range of age t was then determined from the ionization timescale, τ, by $t = \tau/n_e$. Therefore, the elapsed time after the plasma was heated is within (12.000–16.000) yr. The total mass of the plasma M_{total} was estimated by $M_{total} = n_e V m_H = (5–32) M_\odot$, where m_H is the mass of a hydrogen atom. These results are consistent with the expected values for a middle-age SNR.

One of the most detailed studies of middle-age and center-filled thermal emission in a SNR interacting with a dense molecular cloud is the W44 model (Cox et al. 1999; Shelton et al. 1999; Shelton et al. 2004). The proximity to molecular clouds of this SNR suggests that the environmental interstellar matter, where the SNR is propagating, is relatively dense. Using Cox's model we have roughly estimated some dynamical characteristics (i.e., the shock radius R_s and shell velocity v_{shell}) for G337.8−0.1. Assuming an energy for the explosion of ~10^{51} erg, we found that $R_s = (8–10)$ pc and $v_{shell} = (180–200)$ km s^{-1}. These values are consistent with the angular size and range of

distance for the SNR under consideration. Thus, G337.8−0.1 could be, a SNR with characteristics similar to W44.

Finally, we have compared the X-ray luminosity of G337.8−0.1 with other proto-typical mixed-morphology SNRs. The unabsorbed X-ray luminosities in the 0.5–10 keV band of G337.8−0.1 for a range of distance between 7 and 12 kpc is $L_X \sim 4.5 \times 10^{34}$ erg s^{-1} and 1.3×10^{35} erg s^{-1}, respectively. The first value is similar to the X-ray luminosity of W28 ($L_X \sim 6 \times 10^{34}$ erg s^{-1}; Rho & Borkowski 2002), G272.2-3.2 ($L_X \sim 5.2 \times 10^{34}$ erg s^{-1}; Harrus et al. 2001), and Kes 32 ($L_X \sim 3.2 \times 10^{34}$ erg s^{-1}; Vink 2008) for the same energy range. This suggests that a distance around 7 kpc for G337.8−0.1 is most probable.

In summary, in this work we reported the first detection at X-ray wavelengths of the SNR G337.8−0.1. The radio and X-ray properties show that the object displays the three basics attributes found in mixed-morphology SNRs, i.e. centrally filled X-ray morphology with lines in its spectra, a shell-like appearance at radio frequencies, and the absence of a prominent, central, compact source in radio and X-ray energies. If the SNR is indeed propagating in a cloudy medium, the interaction of the shock-front with the adjacent molecular material could be responsible for the gamma-ray emission detected by the EGRET telescope.

The detailed properties of the SNR are still unknown because of the low photon statistics in the XMM-*Newton* data. Future X-ray observations with a higher spatial resolution and good photon statistics like Chandra or Suzaku will reveal the relation between the X-ray intensity peak and the radio emission.

References

Anders, E., & Grevesse, N. 1989, Geochim. Cosmochim. Acta, 53, 197
Arnaud, K. A. 1996, Astronomical Data Analysis Software and Systems V, 101, ASP Conf. Ser., 101, 17
Brickhouse, N. S. 2003, IAUJD, 17, 23
Caswell, J. L., Murray, J. D., Roger, R. S., et al. 1975, A&A, 45, 239
Cowie, L. L., & McKee, C. F. 1977, ApJ, 211, 135
Cox, D. P., Shelton, R. L., Maciejewski, W., et al. 1999, ApJ, 524, 179
Dame, T. M., Elmegreen, B. G., Cohen, R. S., & Thaddeus, P. 1986, ApJ, 305, 892
De Luca, A., & Molendi, S. 2004, A&A, 419, 837
Dickey, J. M., & Lockman, F. J. 1990, ARA&A, 28, 215
Green, A. J., Frail, D. A., Goss, W. M., & Otrupcek, R. 1997, AJ, 114, 2058
Harrus, I. M. 1997, ApJ, 488, 781
Harrus, I. M., Hughes, J. P., Singh, K. P., et al. 2001, ApJ, 552, 614
Hartman, R. C., Bertsch, D. L., Bloom, S. D., et al. 1999, ApJS, 123, 79
Hughes, J. P., Hayashi, I., & Koyama, K. 1998, ApJ, 505, 732
Jones, L. R., Smith, A., & Angelini, L. 1993, MNRAS, 265, 631
Koralesky, B., Frail, D. A., Goss, W. M., et al. 1998, AJ, 116, 1323
Mazzotta, P., Mazzitelli, G., Colafrancesco, S., & Vittorio, N. 1998, A&AS, 133, 403
Morrison, R., & McCammon, D. 1983, ApJ, 270, 119.
Press, W. H., Teukolsky, S. A., Vetterling, W. T., & Flannery, B. P. 1992 (Cambridge: University Press), 2nd edn
Rho, J.-H., & Petre, R. 1996, ApJ, 467, 698
Rho, J., & Petre, R. 1998, ApJ, 503, L167
Rho, J., & Borkowski, K. J. 2002, ApJ, 575, 201
Safi-Harb, S., Dubner, G., Petre, R., et al. 2005, ApJ, 618, 321
Shaver, P. A., & Goss, W. M. 1970, Austr. J. Phys. Astrophys. Suppl., 17, 133
Shelton, R. L., Cox, D. P., Maciejewski, W. S., et al. 1999, ApJ, 524, 192
Slane, P., Smith, R. K., Hughes, J. P., & Petre, R. 2002, ApJ, 564, 284
Strüder, L., Briel, U., Dennerl, K., et al. 2001, A&A, 365, L18
Turner, M. J. L., Abbey, A., Arnaud, M., et al. 2001, A&A, 365, L27
Vink, J. 2004, ApJ, 604, 693
White, R. L., & Long, K. S. 1991, ApJ, 373, 543
Whiteoak, J. B. Z., & Green, A. J. 1996, A&A, 118, 329